Journal of
Ship&Ocean
Technology
©DECEMBER 2005

SOTECH Vol. 9, No. 4, pp. 1 ~ 10, 2005

The Effect of Buoyancy Orientation on Flow Structures in Turbulent Channel Flow using DNS

Osama El-Samni[1], Hyun Sik Yoon[1], Ho Hwan Chun[1]

[1] Advance Ship Engineering Research Center, Pusan National University, Busan, Korean;
E-mail: lesmodel@pusan.ac.kr

Abstract

The effect of buoyancy orientation on turbulent channel flow has been investigated using DNS (direct numerical simulation). Grashof number is kept at 9.6×10^5 while changing the orientation of the buoyancy vector to be parallel or perpendicular to the channel walls. Four study cases can be distinguished during this research namely; streamwise, wall-normal unstable stratification, wall-normal stable stratification and spanwise oriented buoyancy. The driving mean pressure gradient used in all cases is adjusted to keep mass flow rate constant while friction Reynolds number is around 150. At this Grashof number, the skin friction shows decrement in the unstable and stable stratification and increment in the other two cases. Analyses of the changes of flow structure for the four cases are presented highlighting on the mean quantities and second order statistics.

Keywords: buoyancy, turbulent channel flow, DNS, Grashof number

1 Introduction

Density variation due to temperature difference is relevant to many industrial and environmental applications such as heat exchangers and stratified atmospheric boundary layers. Such forces play a significant role in the dynamics of mixed convective flows. Based on the alignment of the buoyancy forces with respect to the bounded walls, different flow configurations may result. Since the buoyancy forces are unidirectional, the position of the walls is the key role in characterizing the resulting flow regimes.

Recently, with the availability of computational resources, direct numerical simulation (DNS) has become a virtual tool in exploring turbulent flows in simple geometries with different body forces. DNS has superiority over the recent experimental techniques mainly because it provides three dimensional instantaneous fields of the resolved quantities and their temporal and spatial correlations of any order. Therefore, DNS can provide detailed budgets of Reynolds stress components, turbulent heat fluxes, temperature variances and dissipation rates of turbulent kinetic energy and temperature variance, which in turn, would be of importance to assess and improve turbulence models used for buoyant flows. Continuous improvements of such models are needed to offer wider applicability and greater complexity of simulating real problems. It has been recognized that buoyant flows has attracted relatively little effort in turbulence modeling improvement due to the scare experimental and numerical data available. Most of the developments done so far were based on DNSs of turbulent natural convection. Readers can refer to the recent articles of Dol et al(1997), Sommer and So(1996), Girimaji and Balachandar(1998) and Dol and

Hanjalić(1999), who used DNS databases generated from Rayleigh-Bénard and vertical natural convection summarized above in the assessment of turbulence models.

Turbulent buoyant channel flow has attracted little attention due to the difficulties associated with the buoyancy and mean shear interactions. Kasagi and Nishimura(1997) studied the turbulent convection in vertical channel where the buoyancy is aligned in the streamwise direction and the flow is upward. The resulting flow showed a distinctive behavior near each wall due to the aiding or opposing effects. Enhancement of Reynolds stress components and wall normal turbulent heat flux was observed in the aiding flow, whereas the suppression of both quantities in the opposing flows. Unstable stratification in horizontal channel can be established when the bottom wall temperature is higher than that of the upper wall. In such case, thermal plumes emerge from the near wall region which had been observed in the DNS of Iida and Kasagi(1997). They attributed the modification of the transport mechanisms to the pressure diffusion and turbulent diffusion. Such thermal plumes work to concentrate the coherent streamwise vortices at the spots where they emerged and therefore they change slightly the low and high speed streaks. On the other hand, stable stratification studied by Iida et al(2002), by switching the temperature boundary conditions, show suppression of turbulence intensities and dominance of internal gravity waves (IGW). The streamwise vortices are concentrated between the IGWs in longitudinally and vertically elongated regions.

Recently, present authors El-Samni et al(2005) have investigated a horizontal turbulent airflow between two vertical plates heated differentially using direct numerical simulation. In this particular configuration, the buoyancy forces result in skewed mean velocity profiles with non-zero anti-symmetric spanwise component. The resulting flow has the features of three-dimensional turbulent boundary layer flows.

The objective of the present study is to explore the different orientations of buoyancy vector with respect to the channel walls on flow structures and consequently on skin friction. The different orientations of buoyant channel flows presented here are shown in Figure 1.

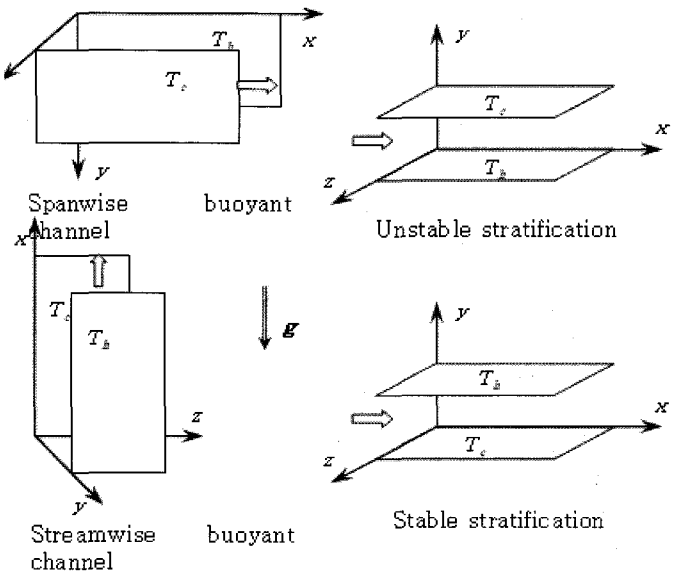

Figure 1: Sketch of the different buoyan 1

2 Computational details

Two differentially heated walls giving sufficient temperature difference to consider the buoyancy effect are proposed for the studied cases as shown in Figure 1. No-slip and no-penetration conditions corresponding to both walls are enforced. The fluid properties are also assumed to be constant, except for the fluid density in the buoyancy term, which follows the Boussinesq approximation. Governing equations describing the instantaneous flow and thermal fields in the present study are the unsteady three-dimensional continuity, momentum and energy equations where the buoyancy term $g\beta(T-T_{ref})$ in each case is added to the momentum equation in the buoyancy direction.

$$\frac{\partial u_i}{\partial x_i} = 0, \tag{1}$$

$$\frac{\partial \boldsymbol{u}_i}{\partial t} + \boldsymbol{u}_j \frac{\partial \boldsymbol{u}_i}{\partial \boldsymbol{x}_j} = -\frac{\mathbf{1}}{\rho}\frac{\partial \boldsymbol{p}}{\partial \boldsymbol{x}_i} + \nu \frac{\partial^2 \boldsymbol{u}_i}{\partial \boldsymbol{x}_j^2} + \boldsymbol{g}_i \delta_{i3} \beta (\boldsymbol{T} - \boldsymbol{T}_{ref}), \tag{2}$$

$$\frac{\partial T}{\partial t} + u_j \frac{\partial T}{\partial x_j} = \alpha \frac{\partial^2 T}{\partial x_j^2} \tag{3}$$

The reference temperature T_{ref} in the present study is assumed to be the mean bulk temperature, which is updated every time step. The variables in the above equations are normalized by the channel half depth δ, friction velocity u_τ and temperature difference between the two walls ΔT. The normalization results in two dimensionless parameters; the friction Reynolds number Re_τ and Grashof number Gr. The Grashof number is fixed at 9.6×10^5 in the present investigations. The driving pressure gradient is adjusted to keep the mass flow rate in the x-direction as constant in all simulations. The computational domain has the dimensions $5\pi\delta \times 2\delta \times 2\pi\delta$ in x-, y- and z-directions, respectively. Those dimensions have been shown to be sufficient to capture the large thermals and plumes in wall bounded flows. Two-point correlations have shown decaying values at separations less than the channel width, which indicates the suitability of the present sizes to give reasonable statistical quantities as discusses by El-Samni et al(2005). The flow is assumed fully developed so that the periodic boundary conditions are simply assigned in the mean flow (x) direction as well as the vertical (z) direction.

Pseudospectral code is used in the simulations of the channel flow. It eliminates the pressure by transforming the Navier-Stokes equations to the vorticity-normal velocity formulation. This technique was originally proposed by Kim et al(1987) in their study of plane channel flow. Fourier series have been used for expanding the resolved variables in the homogenous directions with equally spaced 128 grids in each direction. In the wall-normal (y) direction, an expansion in terms of orthogonal Chebyshev polynomials is employed. Since flow variables are changing only in y-direction, plane averages over x-z planes have been accumulated after reaching fully developed state. The present study shows longer integration period in order to get stationary statistics. Time averaging is made for the two Grashof number cases over a period of $2700\,\nu/u_\tau^2$ which is quite longer than the periods used in generating databases in the other DNS simulations of buoyant channel flows.

The Present simulations are carried out using a Spectral code by El-Samni et al(2005). Comparisons with the previously studied buoyant channel flows show excellent agreements.

3 Results and discussions

The effects of the relative position of the channel wall with respect to the buoyancy vector on the mean streamwise velocity plotted in wall units are compared with the non-buoyant flow as shown in Figure 2. It can be observed that the logarithmic region diminishes in three cases; the unstably stratification(in accordance to the results of Iida and Kasagi (1997) at relatively higher Grashof number of 1.3×10^6), stable stratification in accordance with different Grashof numbers studied by Iida et al(2002) and the aiding side of streamwise buoyancy case.

The corresponding skin friction coefficients normalized by the non-buoyant channel flow are listed in Table 1. It can be seen that stable stratification shows the lowest skin friction among the different orientation cases in accordance to the mean velocity profile shown in Figure 2. It should be mentioned that the unstable stratification case shows also a decrement in the skin friction at moderate Grashof numbers. However with increasing Grashof number the skin friction increases more than the non-buoyant case as indicated by Iida and Kasagi(1997). In the streamwise case, distinctive changes in the skin friction can be observed depending on whether the buoyancy aids or opposes the flow. The lower skin friction is observed in the opposing flow while the aiding flow shows the higher skin friction. In the case where the buoyancy is aligned in the spanwise direction, the normalized skin friction is always increasing.

Figure 3 shows the mean temperature profiles in the wall units for the different orientations. The temperature profile in the spanwise case shows the minimum deviation from the non-buoyant profile preserving the logarithmic region. The logarithmic regions diminish in both the unstable and stable stratification cases. The profile is more laminarized near the aiding side of the streamwise case while the opposing side is shifted downwards showing highly turbulent trend.

Table 1: Normalized skin friction coefficient by the non-buoyant channel C_{f_0}

	Streamwise (Aiding)	**Streamwise (Opposing)**	**Spanwise**	**Unstable stratification**	**Stable stratification**
C_f/C_{f_0}	1.1485	0.9165	1.037	0.9536	0.835

This confirms the difficulty arising in modeling buoyant flows especially when the bounding walls are changing with respect to the gravity vector.

Reynolds stress components are plotted along with the corresponding values of the non-buoyant channel as shown in Figure 4. In the unstable and stable stratification cases, u^+_{rms} u^+_{rms} increases while both v^+_{rms} and w^+_{rms} decrease in the viscous and buffer layers indicating the mechanism of turbulent transport are similar in both cases yet, a distinctive behavior was shown at higher Grashof number in the previous DNS of Iida at al(2002). In this region the energy is transferred to the streamwise component from both spanwise and wall-normal components. Far from the walls, and in the core region, all components are enhanced. In the streamwise case, both walls show different behaviors in near wall region. The opposing wall reveals enhancement for all the three Reynolds stress normal components while the aiding flow shows suppression of those components. In contrast to the stable and unstable stratification, near the wall in the spanwise case, both v^+_{rms} and w^+_{rms} show enhancement while they extract energy from u^+_{rms} component. This can be attributed to the thermal plumes emerge from each wall and move towards to the opposing wall.

Such large-scale structures are associated with the increase in the cross-stream velocities v^+_{rms} and w^+_{rms}. Further away from the wall all components are enhanced. The Reynolds shear stress $-uv^+$ is suppressed in the stable and unstable stratification cases in near wall region. In the streamwise case suppression and enhancement of aiding and opposing flows can be observed in accordance with the changes of the skin friction listed in Table 1. The spanwise case shows a slight difference from that of non-buoyant channel flow. It should be mentioned that the spanwise case among the other studied cases show three-dimensionality and consequently the mean spanwise velocity component and the off diagonal components of Reynolds stress are non-zero.

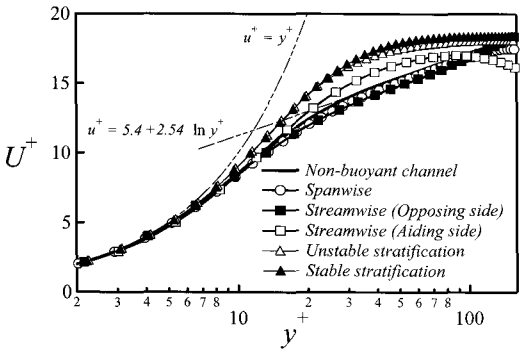

Figure 2: Streamwise mean velocity in wall units

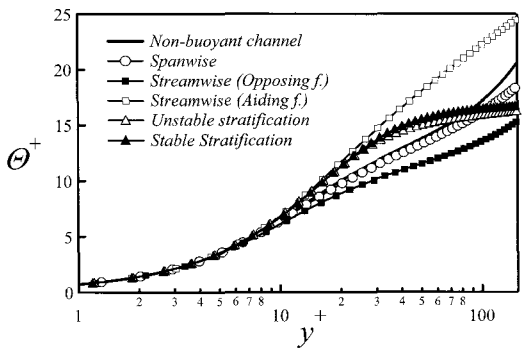

Figure 3: Mean temperature in wall units

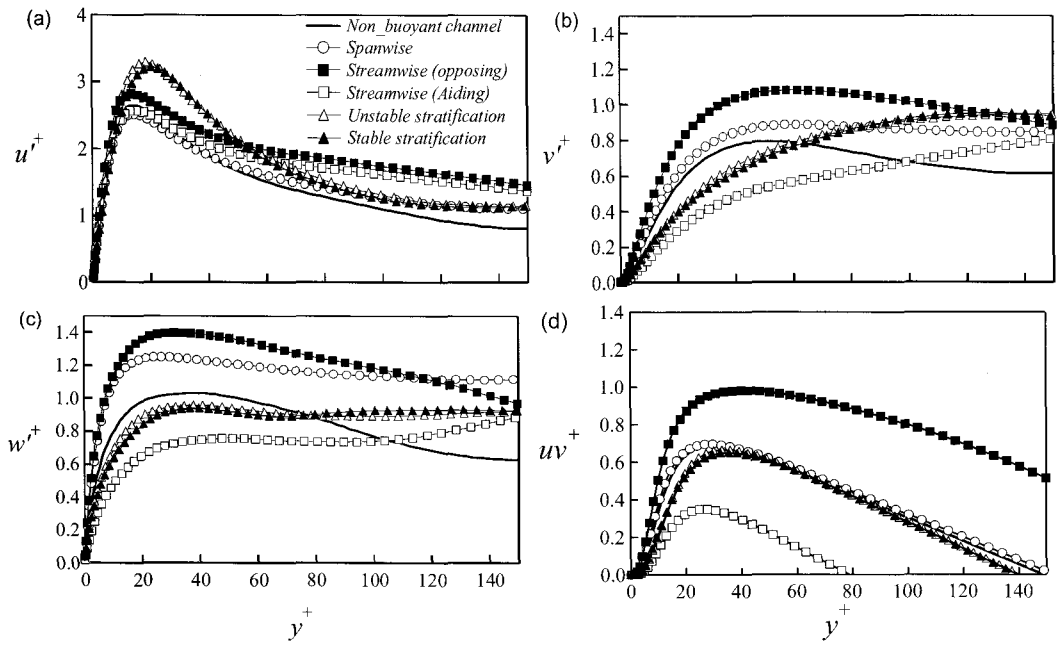

Figure 4: (a) RMS of streamwise component, (b) RMS of wall-normal component, (c) RMS of spanwise component, and (d) Reynolds shear stress.

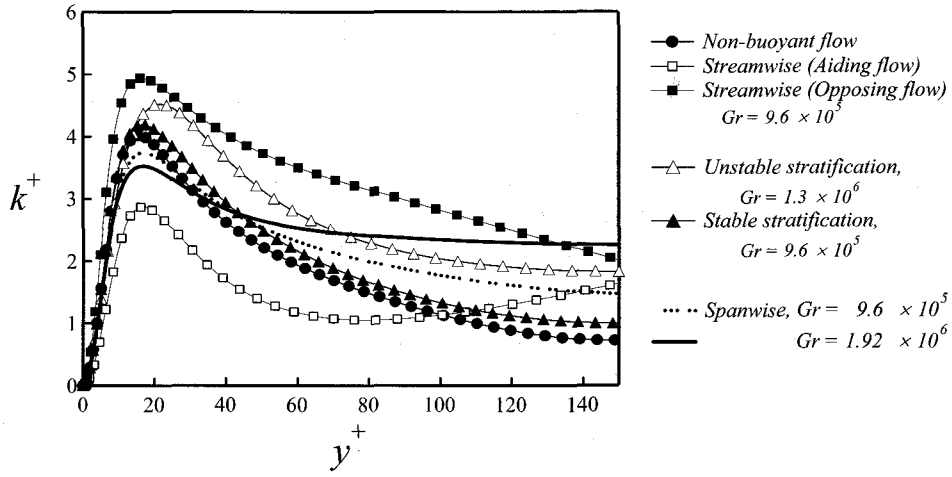

Figure 5: Turbulent kinetic energy at different Grashof numbers and orientations.

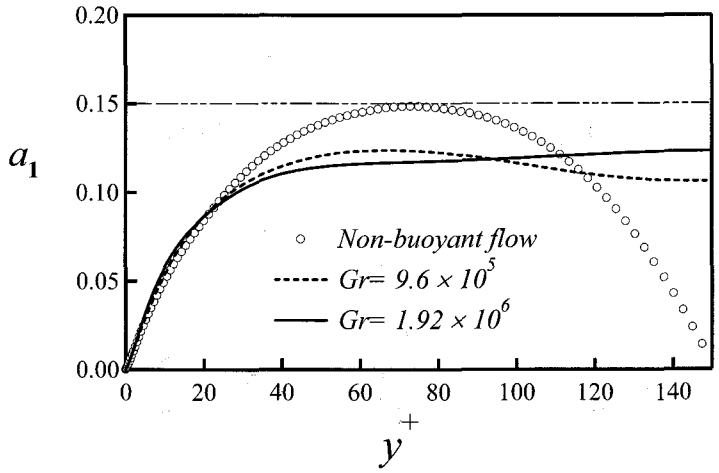

Figure 6: The structure parameter a_1

Turbulent kinetic energy compared with the other orientations is shown in Figure 5. The largest deviation from the non-buoyant channel can be seen in the streamwise case at both walls; the opposing and the aiding sides. While the opposing flow reveals large increase in k^+ due to the rapid increase of u'^2 and w'^2 referred to by Kasagi and Nishimura (1997), the aiding flow shows the maximum reduction. In both stable and unstable stratification cases, k^+ increases with the unstable case revealing higher values than the stable case. In the spanwise case, several observations can be deduced from the current simulation as was discussed in details in El-Samni et al(2005). In the viscous sublayer, there exists a little increase in turbulent kinetic energy with increasing Grashof number. This increase of k^+ in the viscous sublayer is also observed in the opposing flow of streamwise buoyant channel. This trend can be attributed to the large increase of w'^2 as shown previously in Figure 4c. In the buffer layer ($10 < y^+ < 20$), there exists slight decrement in turbulent kinetic energy where the maximum reduction in u'^2 occurs as shown in Figure 4(a).

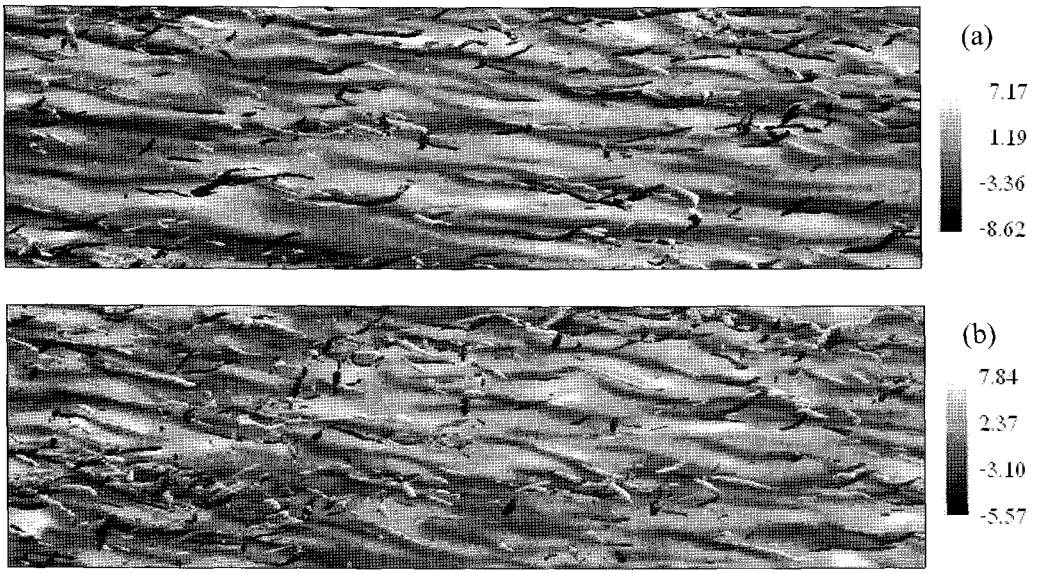

Figure 7: Frontal-view of vortical structures identified by $-\lambda_2$ embedded with the low- and high speed streaks at $y^+ \approx 13$ near the vertical cold wall. (a) $Gr = 9.6 \times 10^5$, $-\lambda^2 = 0.025$ and (b) $Gr = 1.92 \times 10^6$, $-\lambda^2 = 0.035$. White structures correspond to negative ω_x' and dark structures to positive ω_x' and flow from left to right.

The structure parameter a_1, defined as the ratio of the total shear stress magnitude to twice the turbulent kinetic energy, is presented in Figure 6 for the two Grashof numbers studied and the non-buoyant channel flow as well. Similar to most of three dimensional boundary layers, a_1 is smaller than two-dimensional boundary layers. Away from the wall it increases again giving a plateau profile due to the generation of $v'w'$ stress.

The effect of Grashof number on the flow and thermal fields is investigated through different flow visualizations. In the present study, the vortical structures are detected by the negative second largest eigenvalue λ^2 of the tensor $S_{ik}S_{kj} + \Omega_{ik}\Omega_{kj}$ where S_{ij} is the symmetric part of the strain rate tensor $(u_{i,j} - u_{j,i})/2$, and Ω_{ij} is the anti-symmetric part of the strain tensor $(u_{i,j} - u_{j,i})/2$. This identification of vortical structure was proposed by Jeong et al (1997) and has been used widely and successfully in capturing coherent structures in different flow configurations. Selecting the threshold in the present study was selected as twice the maximum RMS of λ^2 in the buffer layer. The iso-surfaces at the lower Grashof number presented in Figure 7a, show little alignment in the z-direction due to the lateral motion. Vortical structures are still organized and tilted with the streaks direction. No indication for concentrations of vortical structures between thermal plumes as was shown in streamwise buoyancy oriented (Kasagi and Nishimura, 1997) and unstable stratification (Iida and Kasagi, 1997) cases. When Grashof number increases, low- and high-speed streaks show larger tilting due to the larger W as shown in Figure 7b. The vortical structures are more disturbed but still they are aligned with the titled streaks. The longitudinal length of the streaks is shown to decrease in the present study and the spacing in the lateral direction is slightly increased as will be shown later. It can be observed from Figure 7b that the pairs of quasi-streamwise vortices have been distorted with one sign of vortex weakened relative to the other. One can recognized the more populated vortices of negative rotation (white iso-surface) than the positive rotating vortices. The negative rotating vortices have been boosted by the mean spanwise strain resulting from the lateral

motion. Such observation is in agreement with the three-dimensional turbulent boundary layer results of Eaton(1995) under the effect of lateral pressure gradient.

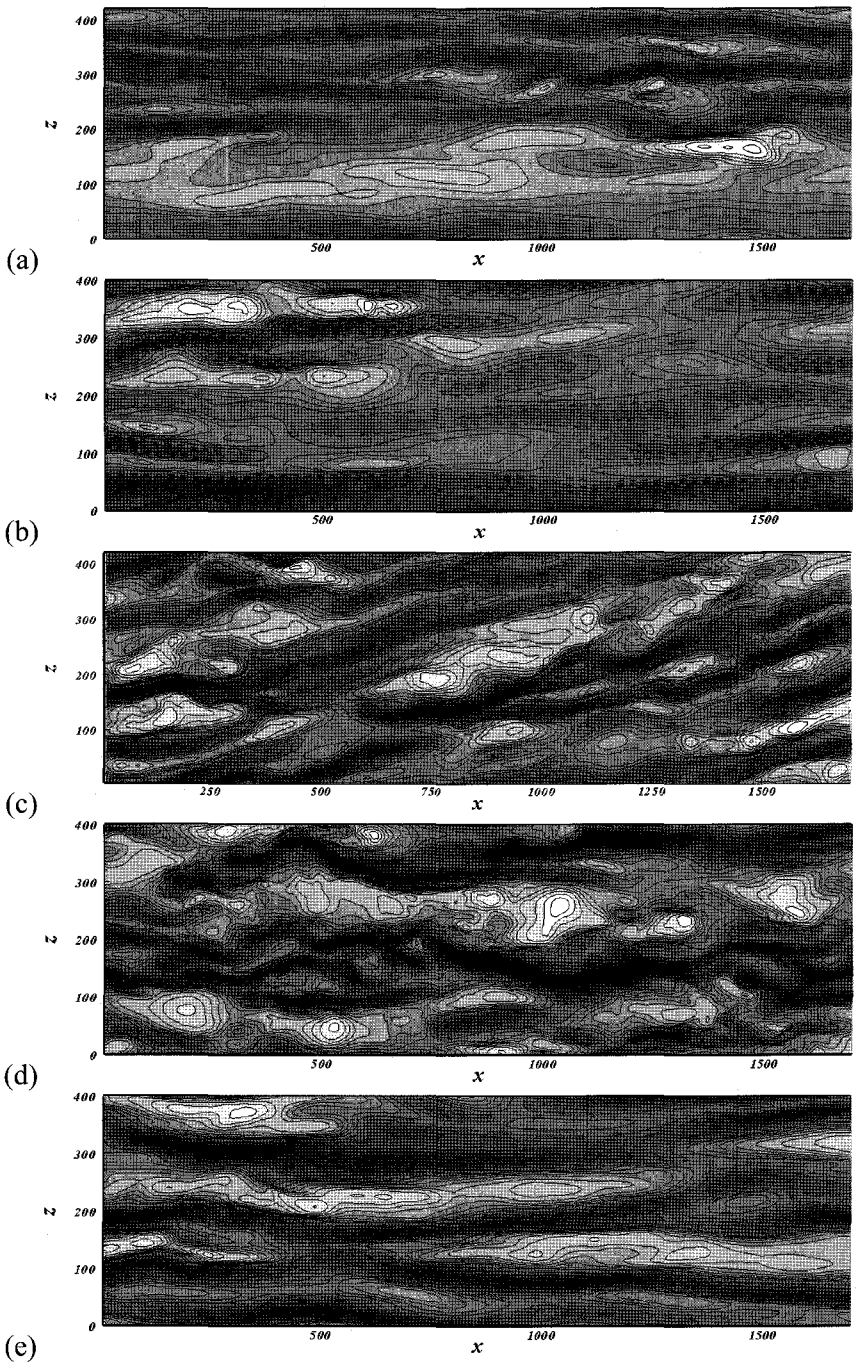

Figure 8: Streaky structures at; (a) unstable stratification, (b) stable stratification, (c) spanwise, (d) streamwise opposing flow and (e) streamwise aiding flow

The streaky structures at distances from the wall of around 13 wall units are compared for each case within the same width z^+ and length x^+ as shown in Figure 8. In the unstable

stratification, there exist wide regions of low and high speed streaks associated with the thermal plumes emerged from near wall region as shown in Figure 8a. Such wide streak spacing results in reducing the ejection and sweep events which in turns, reduce the generation of Reynolds shear stress $-uv^+$. In the stable stratification case shown in Figure 8b, the streaks spacing are around that of non-buoyant flow, yet the strength of the ejection and sweep events are weaker and the flow seems to be laminarized while increasing the Grashof number. In the spanwise case, because of the induced mean spanwise velocity W, the streaks are tilted in the z-direction with little larger spacing than the non-buoyant flow as shown in Figure 8c. In the opposing flow, the streaks become thinner and shorter and stronger meandering than the non-buoyant flow which indicates the activation of vortical structures with smaller sizes and augmentation in shear stress generation as shown in Figure 8d. In the aiding flow shown in Figure 8e, the streaks become thick and longer than those of non-buoyant flow indicating the less activity of vortices and suppression of Reynolds shear stress.

4 Conclusions

Series of DNS have been performed to investigate the effect of buoyancy orientation on turbulent channel flow. When the buoyancy forces are perpendicular to the channel walls, there exists two distinguished cases; the stable and unstable stratification. Since the Grashof number used for comparing those two cases, little difference could be observed. However, the skin friction in the two cases is the lowest among the studied cases. With increasing Grashof number, the turbulence in unstable stratification case is expected to be augmented. When the buoyancy forces are aligned with the flow direction, two opposite effects take place at each wall of the channel. The flow is more activated near the so-called opposing side and suppressed near the other aiding side. When the buoyancy forces are in the spanwise direction, the flow becomes highly three-dimensional where a new induced mean spanwise velocity results in tilting the flow in the lateral direction. The different orientations of the buoyancy vector leads to distinguished behaviors in near-wall streaky structures and the quasi-streamwise vortices.

The study reveals the necessity to consider carefully the buoyancy direction in turbulence modeling of flows of mixed convections. However further investigations for larger Grashof number and detailed statistical analysis of the higher order quantities are needed to obtain clearer understanding of the effect of buoyancy in wall bounded flows which would be of great help and assistance to turbulence modelers and research groups working in the thermal equipment field.

Acknowledgments

This work was supported by Advanced Ship Engineering Research Center (ASERC), Pusan National University, through the Korean Science and Engineering Foundation.

References

Dol, H.S., K. Hanjalić, and S. Kenjereš. 1997. A comparative assessment of the second-moment differential and algebraic models in turbulent natural convection. Int. J. Heat and Fluid Flow, **18**, 4-14.

Dol, H.S., K. Hanjalić, and T.A.M. Versteegh. 1999. A DNS-based thermal second-moment closure for buoyant convection at vertical walls. J. Fluid Mech, **391**, 211-247.

Eaton J.K. 1995. Effects of mean flow three dimensionality on turbulent boundary-layer structure. AIAA J., **33**, 2020-2025.

El-Samni, O.A., H.S. Yoon and H.H. Chun. 2005. Direct numerical simulation of turbulent flow in a vertical channel with buoyancy orthogonal to mean flow. Int. J. Heat Mass Transfer, **48**, 1267-1282.

Girimaji, S.S. and S. Balachandar. 1998. Analysis and modeling of buoyancy-generated turbulence using numerical data. Int. J. Mass and Heat Transfer, **4**, 915-929.

Iida, O. and N. Kasagi. 1997. Direct numerical simulation of unstably stratified turbulent channel flow. ASME Trans. Heat Transfer, **119**, 53-61.

Iida, O., N. Kasagi and Y. Nagano. 2002. Direct numerical simulation of turbulent channel flow under stably density stratification. Int. J. Mass and Heat Transfer, **45**, 1693-1703.

Jeong, j., F. Hussain, W. Schoppa and J. Kim. 1997. Coherent structures near the wall in a turbulent channel flow. J. Fluid Mech., **332**, 185-214.

Kasagi, N. and M. Nishimura. 1997. Direct numerical simulation of combined forced and natural turbulent convection in a vertical plane channel. Int. J. Heat and Fluid Flow, **18**, 88-99.

Kim, J., Moin, P. and Moser, R. 1987. Turbulence statistics in fully developed channel flow at low Reynolds number. J. Fluid Mech., **177**, 133-166.

Sommer, T.P. and R.M.C. So. 1996. Wall-bounded buoyant turbulent flow and its modeling. Int. J. Mass and Heat Transfer, **39**, 3595-3606.